SUPPLEMENTARY INFORMATION

1

One-shot high-resolution melting curve analysis for *KRAS* point-mutation

discrimination on a digital microfluidics platform

*Mingzhong Li,[a] Liang Wan,[ab] Man-Kay Law,[*ab] Li Meng,[ab] Yanwei Jia,[*ab] Pui-In Mak,[ab] and Rui P. Martins[abc]*

[a]State Key Laboratory of Analog and Mixed-Signal VLSI, University of Macau, Macao, China

[b]Faculty of Science and Technology – Electrical and Computer Engineering, University of Macau, Macao, China.

[c]On leave from Instituto Superior Técnico, Universidade de Lisboa, Lisboa, Portugal.

To whom correspondence should be addressed:

[*]Email: mklaw@umac.mo, yanweijia@umac.mo.

Tel.: 00853-8822 8791.

S. Supplementary Information

S1. Fabrication and Assembly Process of the DMF Device

The fabrication and assembly of the DMF devices are conducted inside the clean-room facilities. The electrodes in 2.5×2.5 mm^2 on the top plate are designed using AutoCAD (Autodesk, Inc) with 60-µm clearance from each other. A 2.5-inch ITO glass is patterned with the electrodes with a standard laser-etching method, as shown in Figure S1(T.a). A 50-µm thick polyimide adhesive tape (3M, USA) is deposited as the mask layer on the ITO substrate. As illustrated in Figure S1(T.b), this aims to prevent the secured area from being exposed to the insulator material. A 5-µm thick NOA68 (Norland Products, USA) photoresist is spin coated onto the surface, as depicted in Figure S1(T.c). After that, Figure S1(T.d) shows that the polyimide adhesive tape is removed, and the deposited dielectric layer is ready for curing by UV exposure. The thickness of the dielectric layer is confirmed with a profilometer (D-600, KLA-Tencor). As shown in Figure S1(T.e), an amorphous fluoropolymer hydrophobic layer with 100-nm thickness is deposited on the actuation plate by spin coating the 0.5% Teflon® AF (1601S, Dupont) in perfluorosilane (FC-40, 3M), followed by 180˚C baking on a hot plate for 10 minutes. A 2.5-inch Titanium (Ti) plate with thickness of 1.1 mm and purity of 99.5% is heated at 400 ℃ in a muffle furnace for 1 hour. This directly transforms the Ti surface into a thin-layer Titania (TiO_2), as shown in Figure S1(B.a). Afterwards, the transformed substrate is immersed in a 10-M NaOH solution. Hydrothermal etching is performed at 110 ℃ in a hydrothermal reactor for different durations (1, 3, 5, 7, and 9 hours) to construct an optimal porous surface with hierarchical micro/nano structure for super hydrophobicity, as shown in Figure S1(B.b). The crystal form of the roughened TiO_2 surface is then fully transformed into anatase by annealing treatment at 500 ℃ in a muffle furnace for 1 hour. This

(T.a) Substrate with Patterned ITO

(B.a) Titania (TiO$_2$) Substrate

(T.b) Mask Layer Deposition

(B.b) Hydrothermal Treatment

(T.c) Dielectric Layer Deposition

(B.c) Silane Treatment

(T.d) Exposure

(B.d) Exposure

(T.e) Hydrophobic Layer Deposition

(B.e) Wettability Patterning

(I) Device Assembly
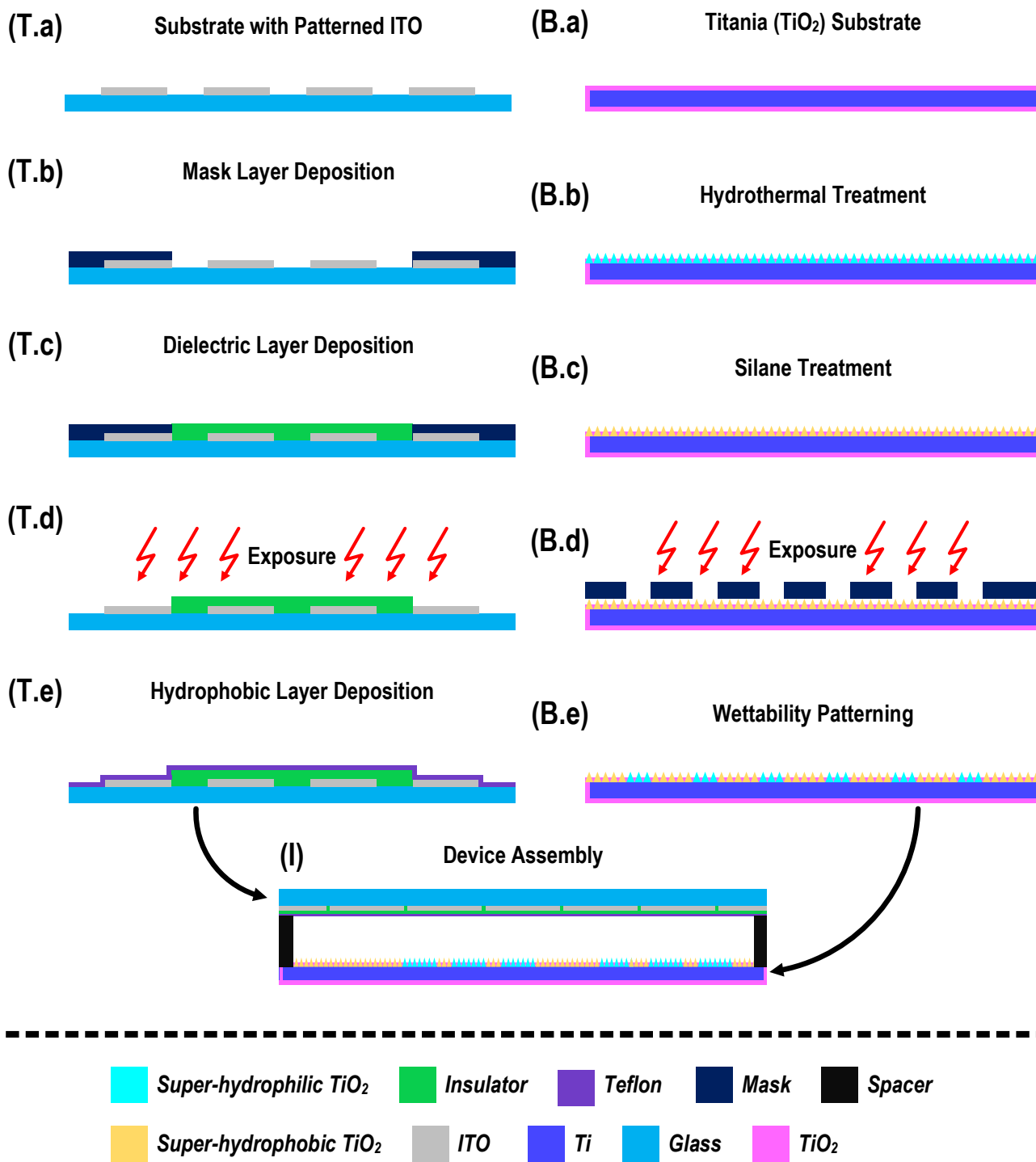
Legend:
Super-hydrophilic TiO$_2$ | Insulator | Teflon | Mask | Spacer
Super-hydrophobic TiO$_2$ | ITO | Ti | Glass | TiO$_2$

Figure S1. Fabrication and assembly of the DMF device. The actuation plate is fabricated layer-by-layer in sequence (T.a-T.e), while the functional plate is prepared on the surface of titanium substrate (B.a-B.e). The assembled DMF device with spacer, actuation and functional plates is illustrated in (I).

renders the surface a structural basis in achieving high-level of oxidation. As shown in Figure S1(B.c),

1   the substrate is further modified with a superhydrophobic monolayer of Trichloro(1H,1H,2H,2H-

2   perfluorooctyl)silane by chemical vapor deposition (CVD) at 200 ℃ in an oven for 30 minutes. After

3   cooling to room temperature, the substrate can be observed superhydrophobic with a contact angle of >

4   170˚ and a sliding angle of < 1˚. Taking advantage of the high-level oxidation, the anatase TiO_2

5   decomposes the superhydrpphobic monolayer by irradiation of the collimated near-ultraviolet light

6   (NUV, 365-436 nm) for 30 minutes. As shown in Figure S1(B.d, B.e), super-hydrophilic patterns are

7   selectively formulated within the super-hydrophobic substrate. A 300-μm thick glass is used as the

8   device spacer to confine the gap height between the actuation and functional plates with the

9   (super)hydrophobic layers facing each other. NOA68 photoresist also plays an adhesive to assemble

10   the whole device as shown in Figure S1(I). Surface treatment using oxygen plasma (Harrick Plasma)

11   is performed prior to the coating of each individual layer.

12   For those as-prepared substrates using the same fabrication procedures and being preserved for over 6

13   months, the changes of the contact angles in air and in hexadecane are illustrated in Table S1. As

14   observed, the contact angles are consistent, and the lifetime of the super-wettability

15   (hydrophobic/hydrophilic) patterns should be at least 6 months.

	Contact Angles in Air		Contact Angles in Hexadecane	
	Hydrophobic	Hydrophilic	Hydrophobic	Hydrophilic
Newly prepared	173°±2.2°	2.32°±0.33°	113°±0.51°	1.5°±0.31°
Over 6 months	164°±2.8°	2.61°±0.29°	105°±0.43°	2.1°±0.52°

16   **Table S1.** Variations of contact angles are measured in air/Hexadecane for over 6 months.

17   **S2. DMF Electronics**

18   The real-time controller of the electronic interface is implemented in Verilog on a DE0-Nano board
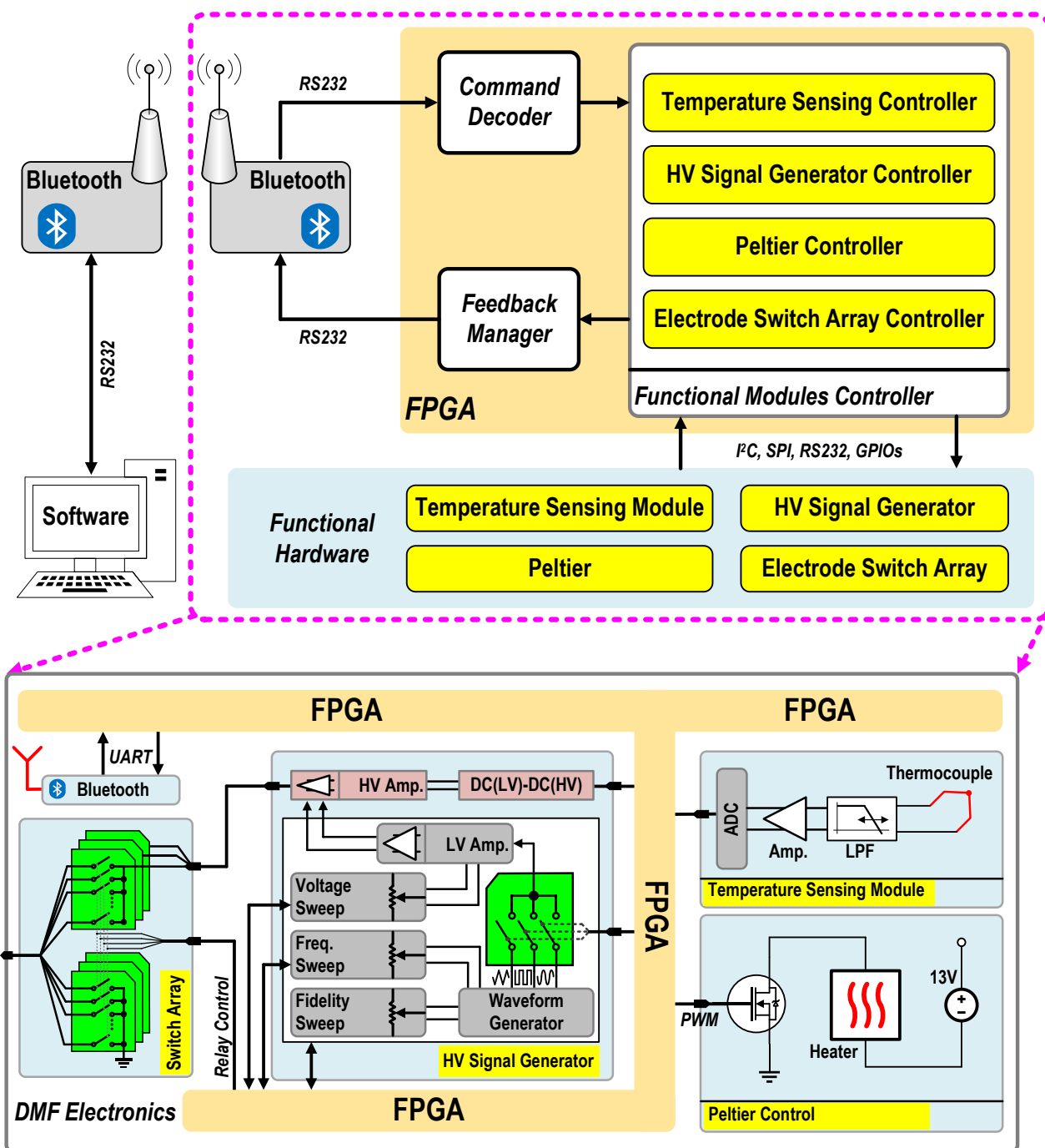
Figure S2. Hardware implementation for the DMF device control.

(Altera Cyclone® IV EP4CE22F17C6N). The field programmable gate array (FPGA) communicates

with the host computer through Bluetooth modules, and manipulates all the hardware by GPIO ports,

I^2C, SPI and RS232. The implementations of the DMF electronics for DMF device interface are

detailed in Figure S2, including the functional hardware modules and corresponding controllers

1   embedded in the FPGA.

2   All the functional modules controllers operate in parallel, with each designed for a specific task. The

3   command receiver acquires the data packaged from the RS232 port and distributes the decoded

4   command to the corresponding functional modules, including the temperature sensing block, high-

5   voltage signal generator, peltier and electrode switch array. The data collected from the functional

6   modules are also encoded, buffered, and transmitted to the host PC through the feedback manager.

7   For the functional modules, the *Electrode Switch Array Controller* operates the IO extenders

8   (MCP23S17-T) through an I^2C interface to manage the multi-channel electrode switching Activities.

9   The *HV Signal Generator Controller* operates the digital potentiometers through SPI interfaces to

10   adjust the output waveform of the high-voltage actuation signal, such as voltage amplitude, and

11   frequency. The *Temperature Sensing Controller* operates the analog-to-digital converter

12   (ADC128S022) on the DE0-nano board to digitize the temperature-dependent voltage signal. In the

13   *Peltier Controller*, pulse width modulation (PWM) is implemented to control the CMOS switching

14   activities for regulating the Peltier temperature. Both the temperature sensing block and Peltier serve

15   to regulate the melting temperature within the device chamber.

16   **S3. Software Program**

17   As shown in Figure S3, the customized software (written in C# and compiled in Microsoft® Visual

18   Studio®) serves as the on-line DMF chip control. The control program is composed of four user

19   interfaces (UI), including the wireless connection UI, electrode actuation UI, hardware configuration

20   UI, and the temperature sensing and control UI as depicted in Figure S3. Detail implementation and

21   functions of these interfaces are discussed in the following sections.

S3.1. Wireless Connection UI

This interface defines the wireless Bluetooth connection between the host computer and the electronic hardware. The serial communication port (COM) reports the real-time connection status and adjusts the corresponding baud rate as demanded.

S3.2. Electrode Actuation UI

Each individual electrode on the DMF chip can be actuated/grounded simultaneously. This could be achieved by either selecting the corresponding UI buttons of specific electrodes or exerting a customized command sequence.

S3.3. Hardware Configuration UI

Parameters settings for the DMF control electronics or FPGA are controlled by the software, including the ADC sampling rate for the temperature sensing module and digital potentiometers for the HV signal generator.

S3.4. Temperature Sensing and Control UI

A close-loop feedback controller is implemented to regulate the DMF operating temperature. The digitized temperature signal from the ADC is sent to host computer for further temperature mapping according to the hardware configurations. Based on the difference between the target and detected ambient temperatures, PWM coefficients are calculated by a proportion-integral-derivative (PID) algorithm and transmitted to the PWM module on the FPGA to regulate the distributed power into the heating membrane. The PWM duty cycle (DC) can be calculated using (1) to (4).

$$DC[n] = DC[n-1] + K_p * E[n] + K_d * DE[n] + K_i * IE[n] \qquad (1)$$

1 $$E[n] = T_{target} - T[n] \tag{2}$$

2 $$DE[n] = T[n-1] - T[n] \tag{3}$$

3 $$IE[n] = T_{target} * m - \sum_{i=n-m}^{n} T[n] \tag{4}$$

4 where n denotes the index of data, T_{target} is the target temperature, $T[n]$ is the nth detected

5 temperature, m is a constant coefficient (set as 15 in our experiment) representing the integration

6 length, and K_p, K_d, K_i are the coefficients for the proportional term ($E[n]$), integral term ($IE[n]$), and

7 derivative term ($DE[n]$), respectively.

Figure S3. Software program for on-line DMF device control.
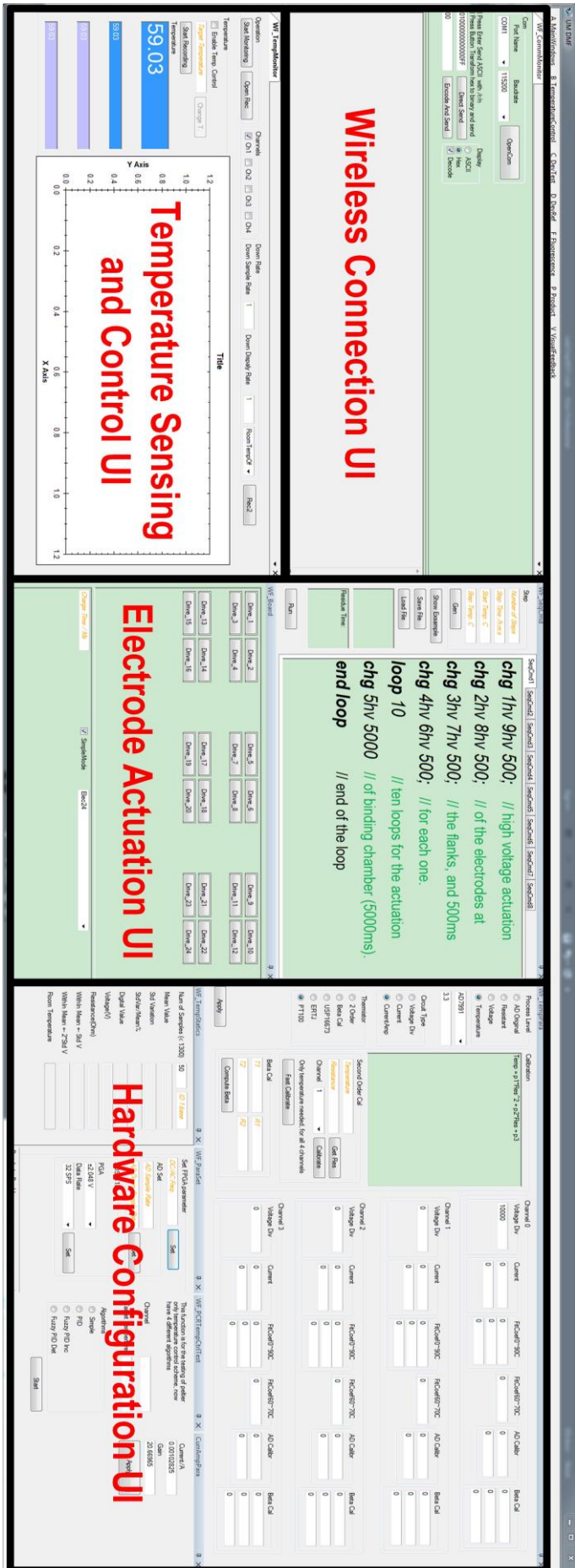
1   **S4. System Configuration**

2   Figure S4 illustrates the experimental configurations. The DMF device is placed on the customized

3   device holder and connected with the DMF electronics. All the electronics are supplied by a standard

4   power bank. The host computer controls all the DMF electronics using the customized software. The

5   experiments are recorded by the fluorescence microscope and the thermal imager.
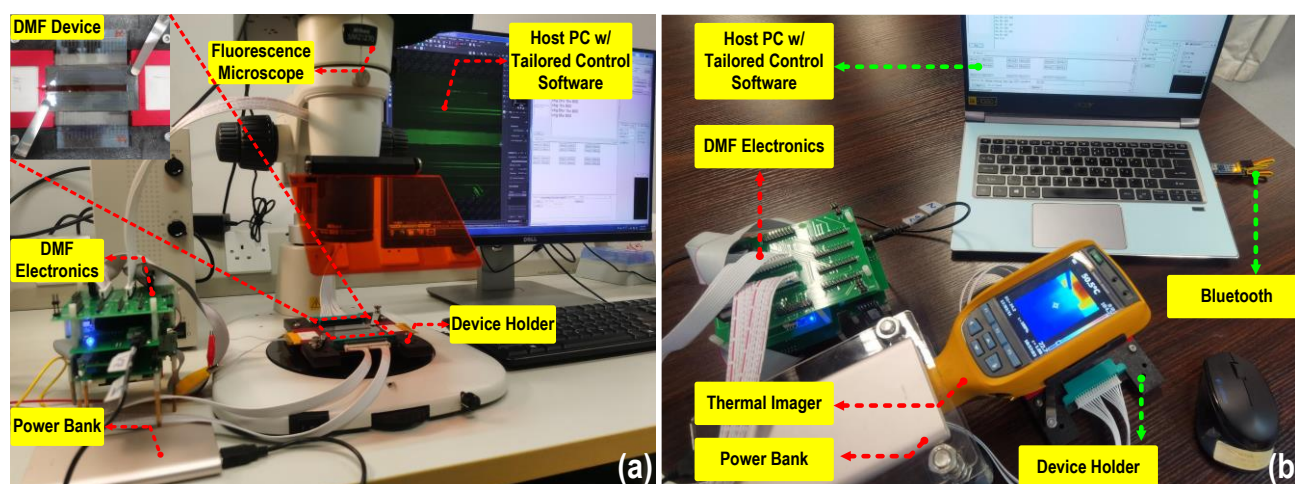
6

7   **Figure S4.** Experimental system configurations with (a) fluorescence microscope, and (b) thermal imager.

8   **S5. Effect of Wettability Contrast on MCA**

9   The surface wettability of the substrate is programmable by regulating the UV photocatalysis

10   time. Even though different wettability contrasts (ΔCA) that are capable of patterning high-

11   resolution droplets can be considered as potential solutions for MCA, the supreme wettability

12   contrast is selected as the optimal scheme in this work. A smaller ΔCA undermines the

13   uniformity of the droplet array, which can affect the MCA accuracy. Figure S5(a, b, e, f)

14   illustrate the T_m of 58.77±0.08 °C for K2 with $\Delta CA=170°$, while the T_m with $\Delta CA=138°$ is

15   58.79±0.46 °C, as shown in Figure S5(c, d, g, h).
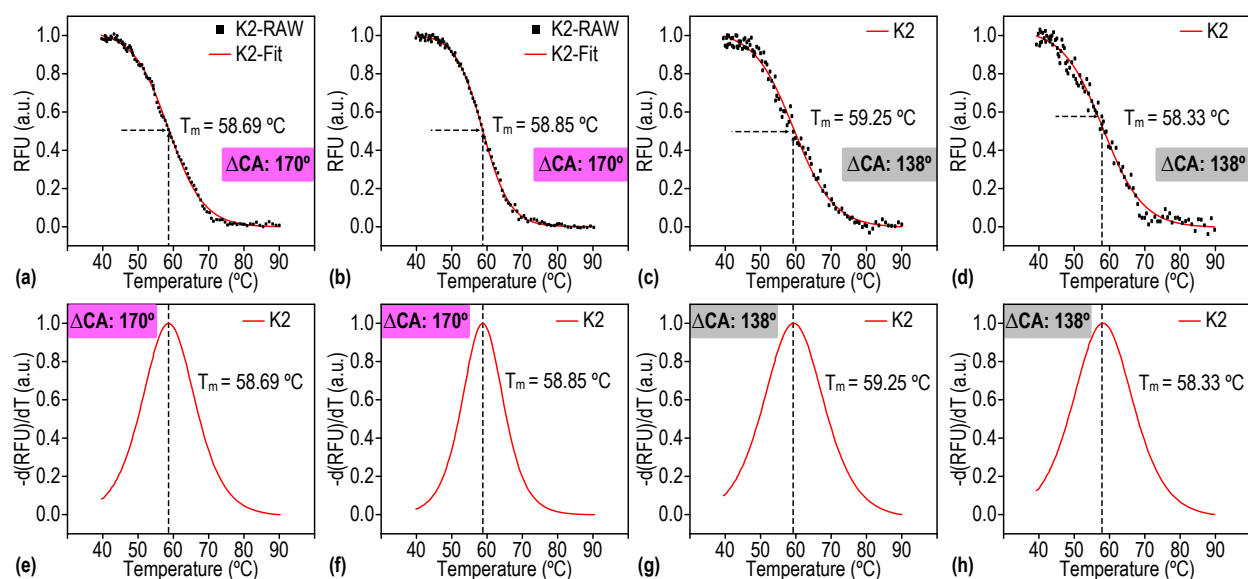
Figure S5. Experimental results illustrating the melting curves and melting peaks with the ΔCA of 170° and 138°, respectively.

S6. Effect of Surface Adsorption

To avoid surface adsorption, we have involved additive reagent in the sample solutions to inhibit the DNA adsorption effect on MCA. We select a mutant-type KRAS gene target (K2) as an example to demonstrate the adsorption effect. A 5-µL mother droplet containing 10-µM K2 is swept across the droplet array for multiple seeding cycles between the inlet and outlet. We retain the mother droplet on each electrode for a fixed time of 5 seconds for observing the surface adsorption effect. Figure S6 shows the corresponding experimental results. As BSA and Tween-20 reduce the surface adsorption and DNA loss, the obtained melting temperatures from 1, 5, and 10 seeding cycles fluctuate with minor differences, with T_m reported as 58.44 °C, 58.78 °C, and 58.49 °C, respectively. This indicates that the surface adsorption presents negligible effect on the MCA results.
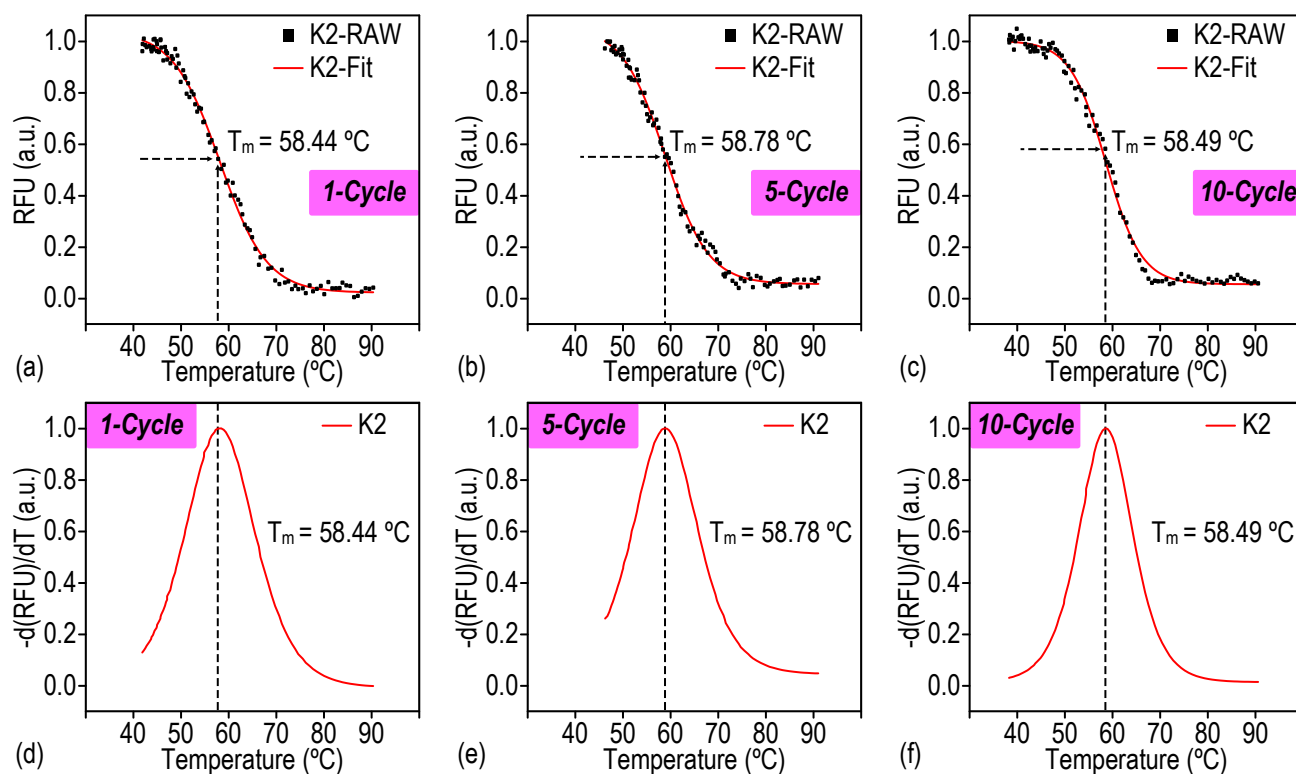
Figure S6. Experimental results illustrate the MCA tests for mutant-type KRAS gene target (K2) with different seeding cycles for the investigation of surface adsorption. (a, b, c) the on-chip melting curves, and (d, e, f) the melting peaks show that that the T_m values of K2 are 58.44 °C, 58.78 °C, and 58.49 °C from 1, 5, and 10 seeding cycles, respectively.

S7. Effect of Fluid Convection

Due to the temperature gradient, fluid convection in the background oil should be theoretically established along the MCA chamber. However, this phenomenon cannot be directly observed due to the transparent and uniform oil phase. In fact, the degree of convection can be reflected and characterized from the movement velocity of the mother droplet. Figure S7(a) illustrates the droplet velocity across 18 electrodes (E1-E18) on the top plate and 101 super-hydrophilic patterns on the functional bottom plate with an actuation voltage fixed at 200 V_{rms} (500 Hz). The velocity is defined as W_E/t, where W_E is the electrode width, and t is motion time for a droplet to move across two adjacent electrodes.

1   We can experimentally observe a varying degree of resistance against the mother droplet movement

2   before and after the thermal equilibrium is established. This effect is more severe when the mother

3   droplet crosses the hot zone where a significant degradation in the droplet velocity is observed, as

4   shown in Figure S7(b). On the contrary, upon thermal equilibrium, the droplet motion velocity is

5   almost constant along the whole temperature gradient. This indicates that the establishment of the

6   thermal equilibrium can reduce the convection effect of the background oil.
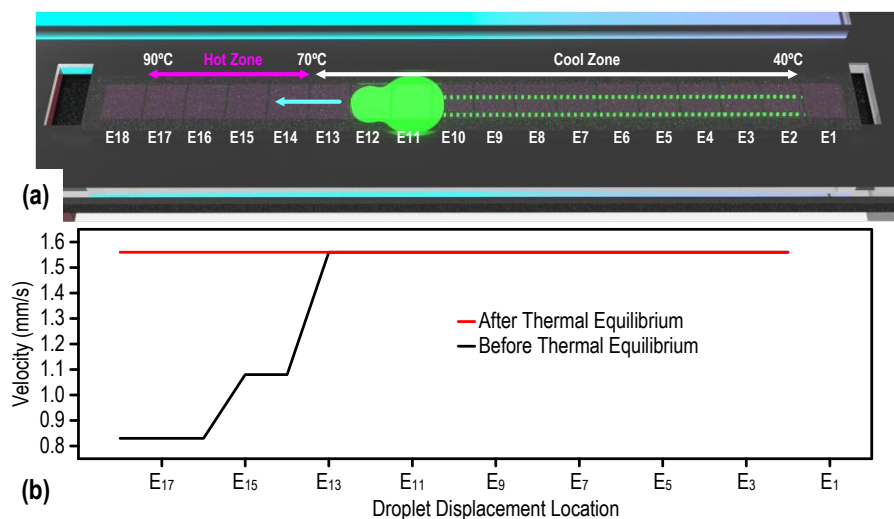
7

8   **Figure S7.** Motion velocity of mother droplet actuated from cool zone to hot zone.

9   **S8. Effect of DNA concentrations and dispensing temperature**

10   The impact of DNA concentrations and dispensing temperature is also studied concerning the melting

11   temperatures. Figure S8 to S10 illustrate the melting curves and melting peaks of K2 samples with

12   various DNA concentrations ranging from 3 µM, 5 µM, and 10 µM. And Figure S11 illustrates the

13   melting curves and their derivatives of 10-µM K2 and K1 as dispensed at room temperature.
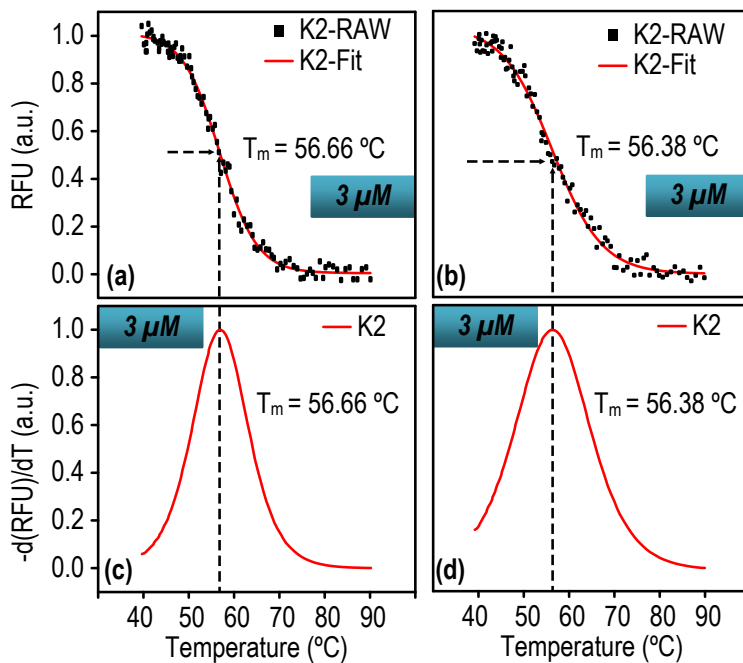
Figure S8. The melting curves and their derivatives of 3-µM K2 are investigated with T_m of 56.32 ± 0.14 °C.

Noted that the microarray is dispensed in the presence of a thermal gradient.
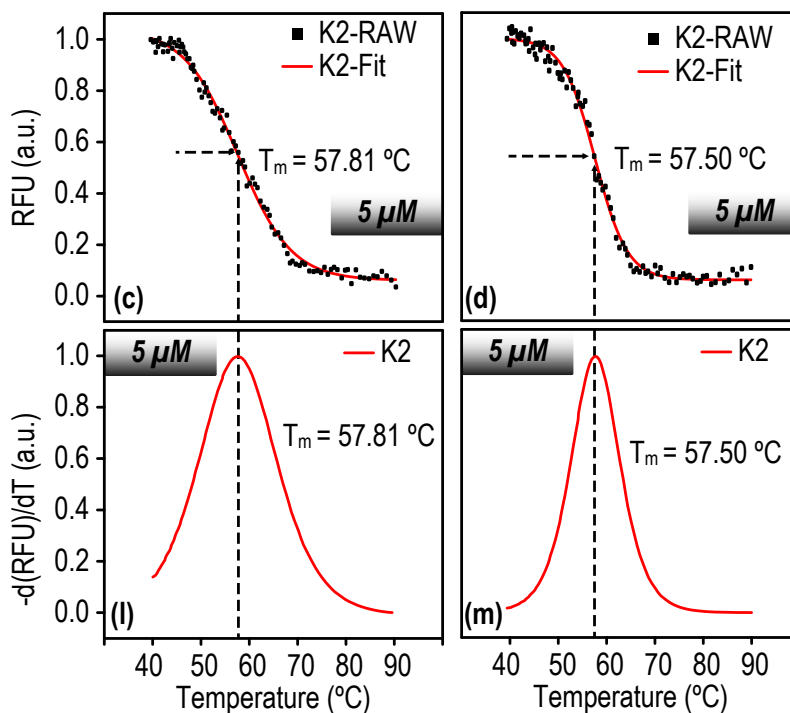
Figure S9. The melting curves and their derivatives of 5-µM K2 are investigated with T_m of $57.655 \pm$ 0.155 °C. Noted that the microarray is dispensed in the presence of thermal gradient.
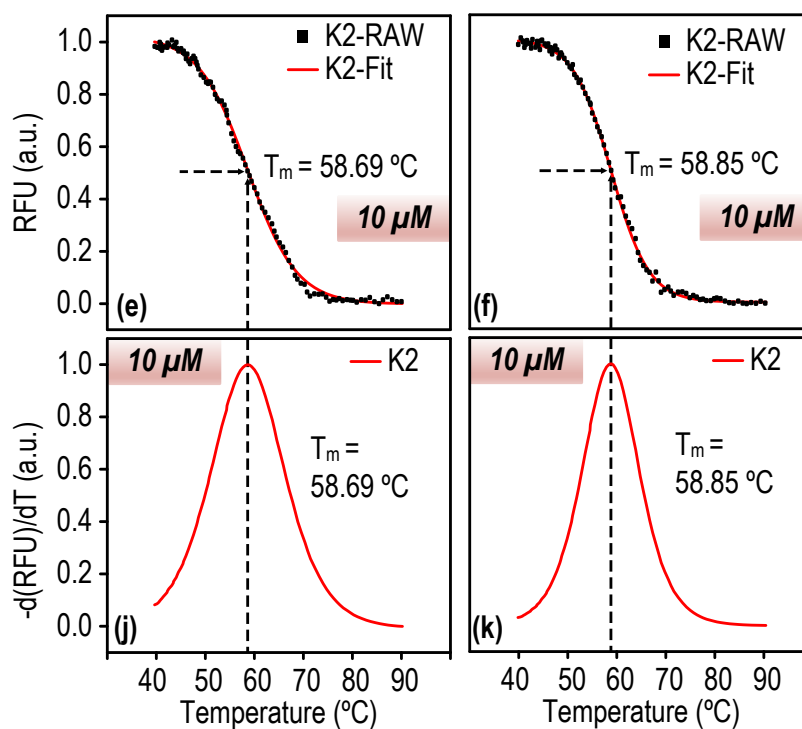
Figure S10. The melting curves and their derivatives of 10-μM K2 are investigated with T_m of 58.77±0.08 °C.

Noted that the microarray is dispensed in the presence of a thermal gradient.
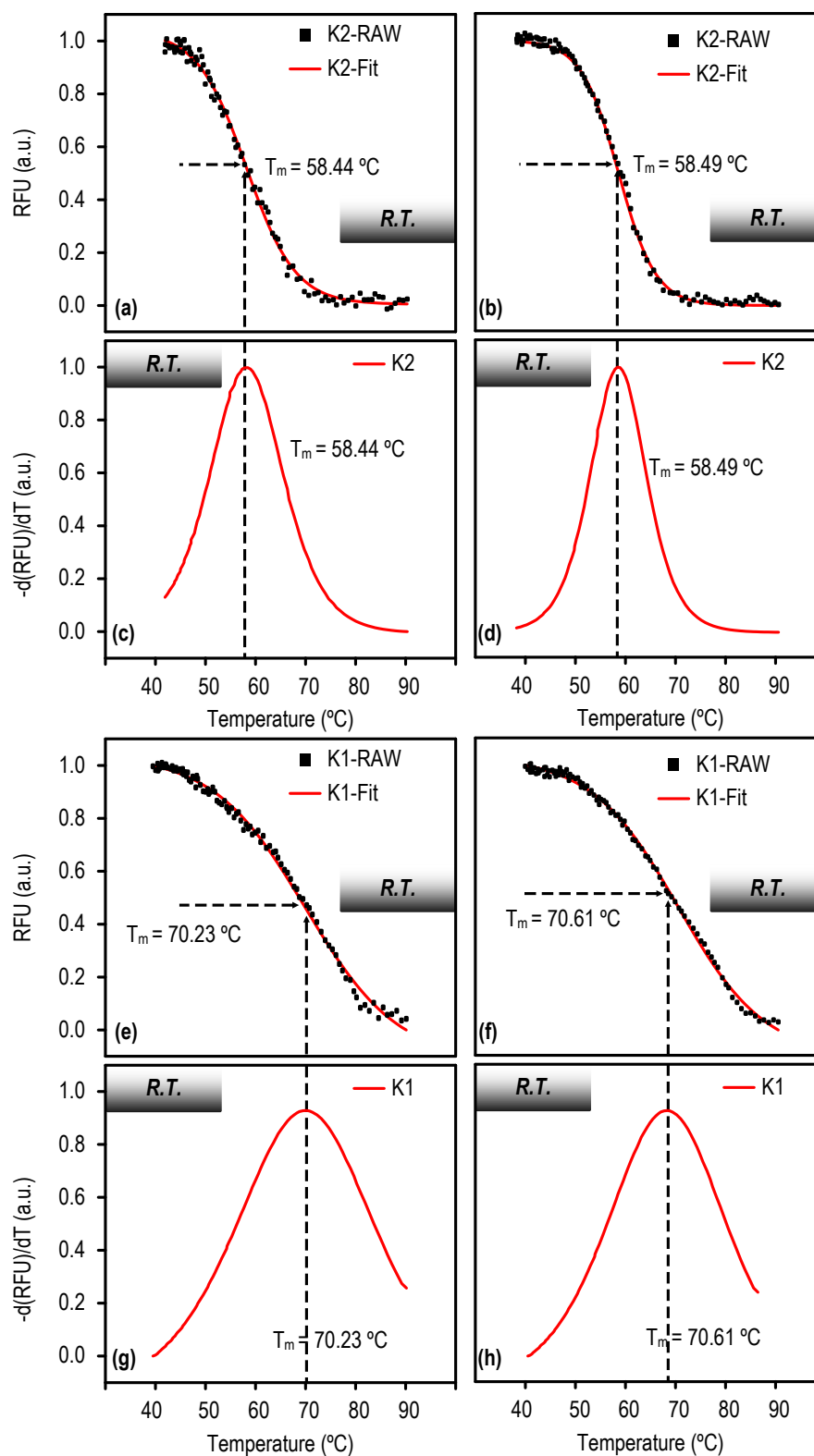
Figure S11. The melting curves and their derivatives of 10-μM K2 and K1 are investigated with T_m of 58.47±0.03 °C and 70.42±0.19 °C. Noted that the microarray is dispensed in the presence of room temperature.

1   **S9. Off-chip and on-chip melting curve analysis**

2   For an on-chip melting curve analysis, a 5-µL DNA mix solution is loaded and actuated in hexadecane

3   oil phase across the substrate, which allows for the isolation of nL-scale samples on the super-

4   hydrophilic patterns. The remaining sample is collected and recycled via the chamber outlet. With an

5   established thermal gradient from 40 °C to 90 °C, the melting curves are obtained from the

6   fluorescence microscope by single exposure for the analysis of melting peaks and melting temperatures.

7   The on-chip measurements for each MCA test are repeated for three times from different microchips.

8   In an off-chip MCA, a total volume of 10-µL the same master mix solution with the on-chip MCA is

9   prepared and evaluated in Bio-Rad CFX96^{TM} Real-Time PCR Detection System (Bio-Rad, USA). The

10 samples are incubated at 95 °C for 2 minutes and 25 °C for 5 minutes, followed by a thermal scanning

11 from 40 °C to 90 °C with an interval of 1 °C for 30 seconds. The off-chip MCA tests are also repeated

12 for three time from different tubes. The off-chip melting curves and derivative plots in Figure (S12-

13 S15) indicate that the melting temperatures of the wild-type and mutant-type *KRAS* gene targets are

14 $T_{m, K1\text{-}GGT}$ = 71.0 °C, $T_{m, K2\text{-}GAT}$ = 59.0 °C, $T_{m, K3\text{-}GCT}$ = 58.0 °C, and $T_{m, K4\text{-}GTT}$ = 58.0 °C, respectively.

15 And the on-chip melting temperatures of the *KRAS* gene targets are $T_{m, K1\text{-}GGT}$ = 69.79±0.22 °C, $T_{m, K2\text{-}GAT}$

16 $_{GAT}$ = 58.76±0.08 °C, $T_{m, K3\text{-}GCT}$ = 57.81±0.06 °C, and $T_{m, K4\text{-}GTT}$ = 58.23±0.08 °C, respectively. Notice

17 that this work only obtains discrete points for the fluorescence-temperature curve. The errors in the

18 melting temperature T_m can occur if the curve fitting result is used. In this work, we mainly employ

19 the fitted curve to figure out the temperature ($T_{m.fit}$) with the largest slope point of the fitted melting

20 curve. We then identify the T_m as the temperature of the adjacent raw data point nearest to $T_{m.fit}$.
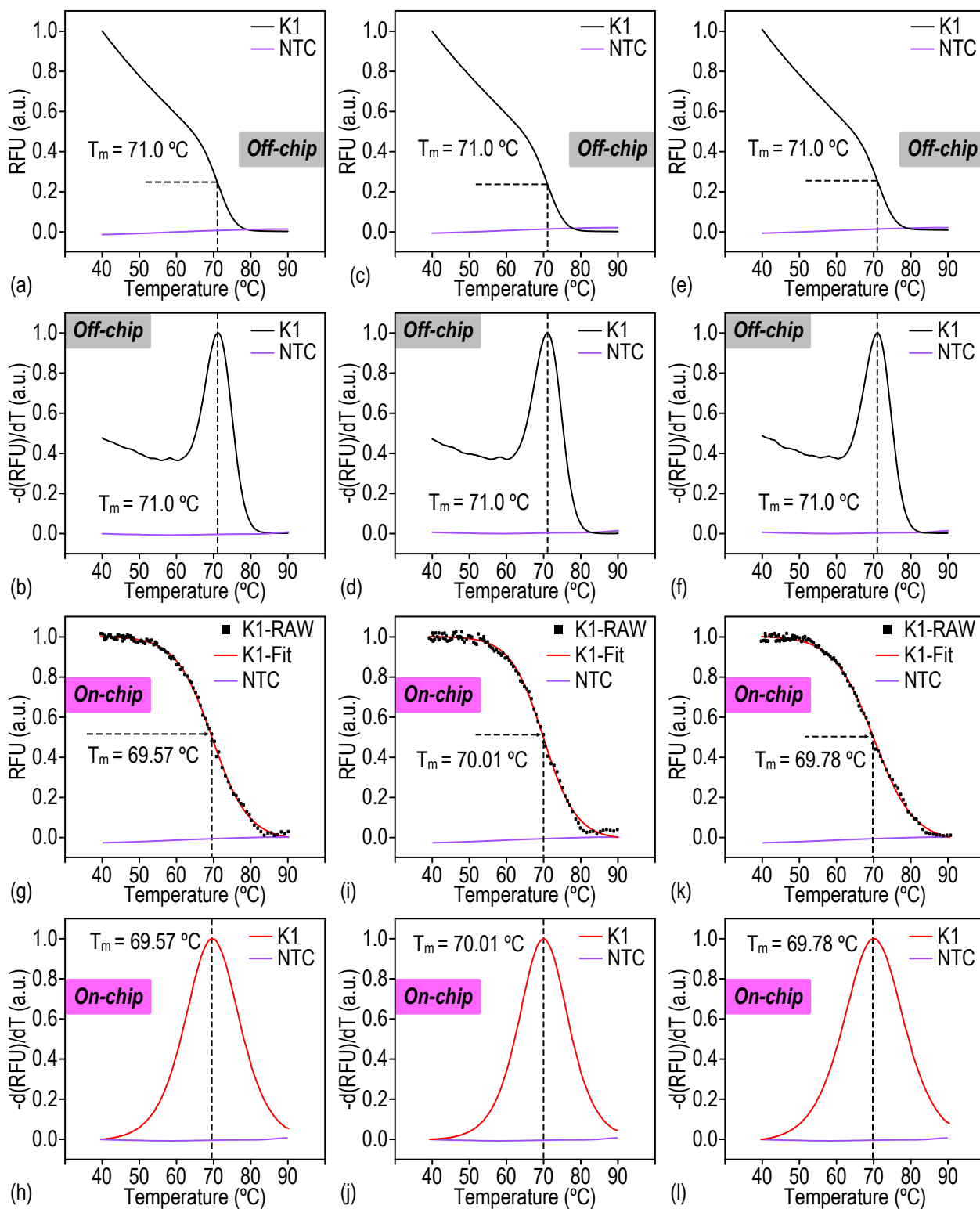
Figure S12. Experimental results illustrate the MCA tests for wild-type KRAS gene target (K1). (a, c, e) the off-chip melting curves, and (g, i, k) the on-chip melting curves. (b, d, f) and (h, j, l) demonstrate the off-chip and on-chip melting peaks, respectively.
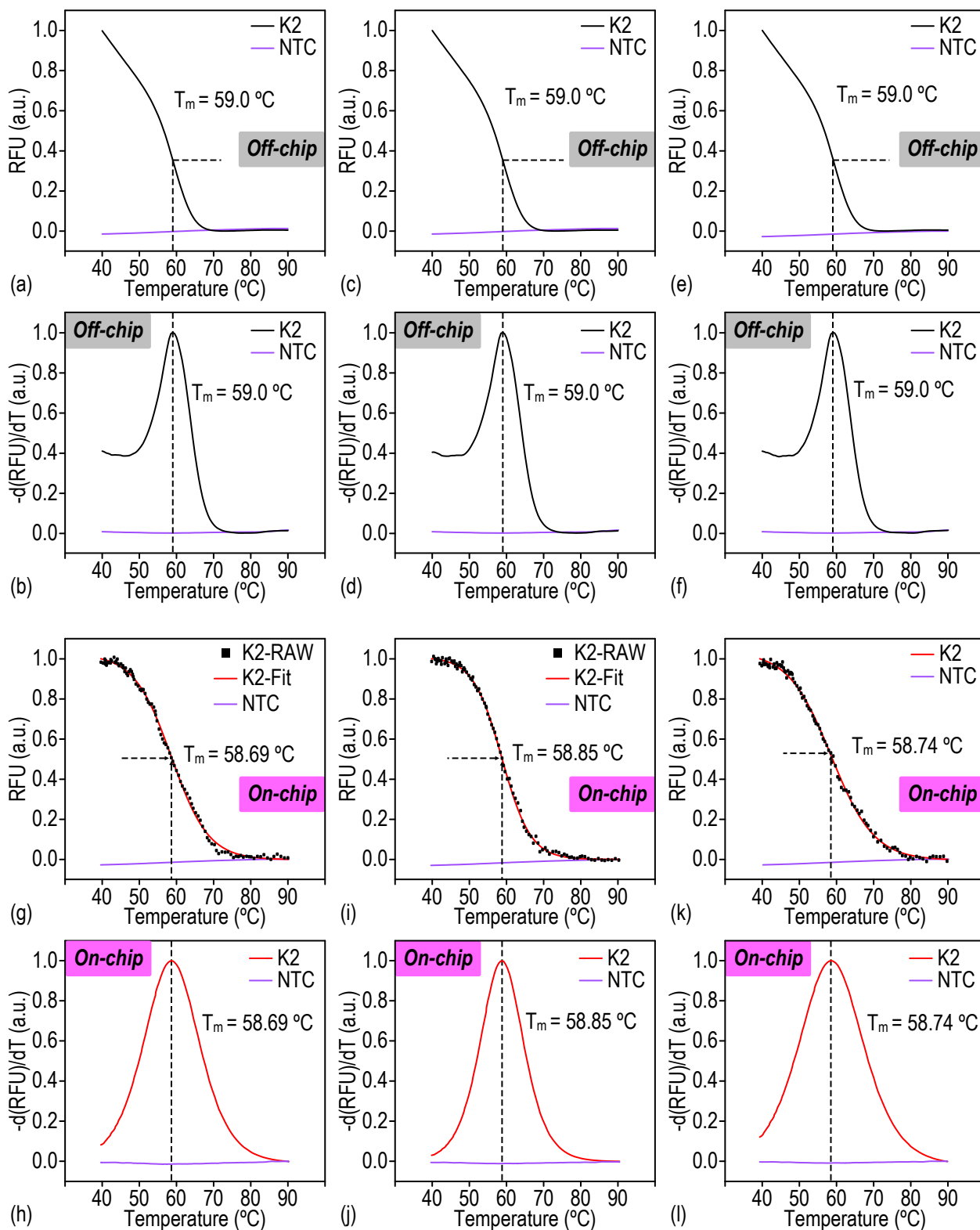
Figure S13. Experimental results illustrate the MCA tests for mutant-type KRAS gene target (K2). (a, c, e) the off-chip melting curves, and (g, i, k) the on-chip melting curves. (b, d, f) and (h, j, l) demonstrate the off-chip and on-chip melting peaks, respectively.
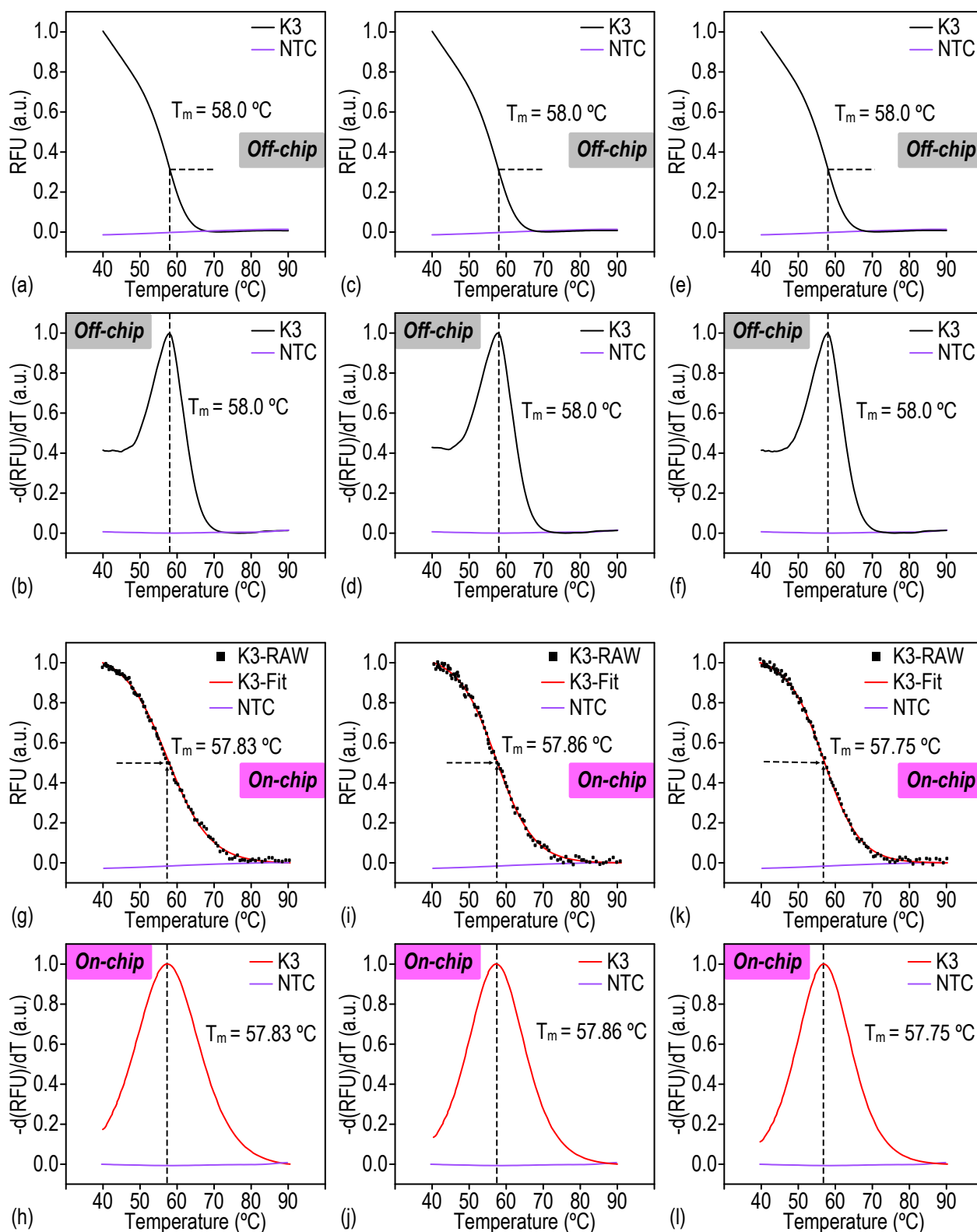
Figure S14. Experimental results illustrate the MCA tests for mutant-type KRAS gene target (K3). (a, c, e) the off-chip melting curves, and (g, i, k) the on-chip melting curves. (b, d, f) and (h, j, l) demonstrate the off-chip and on-chip melting peaks, respectively.
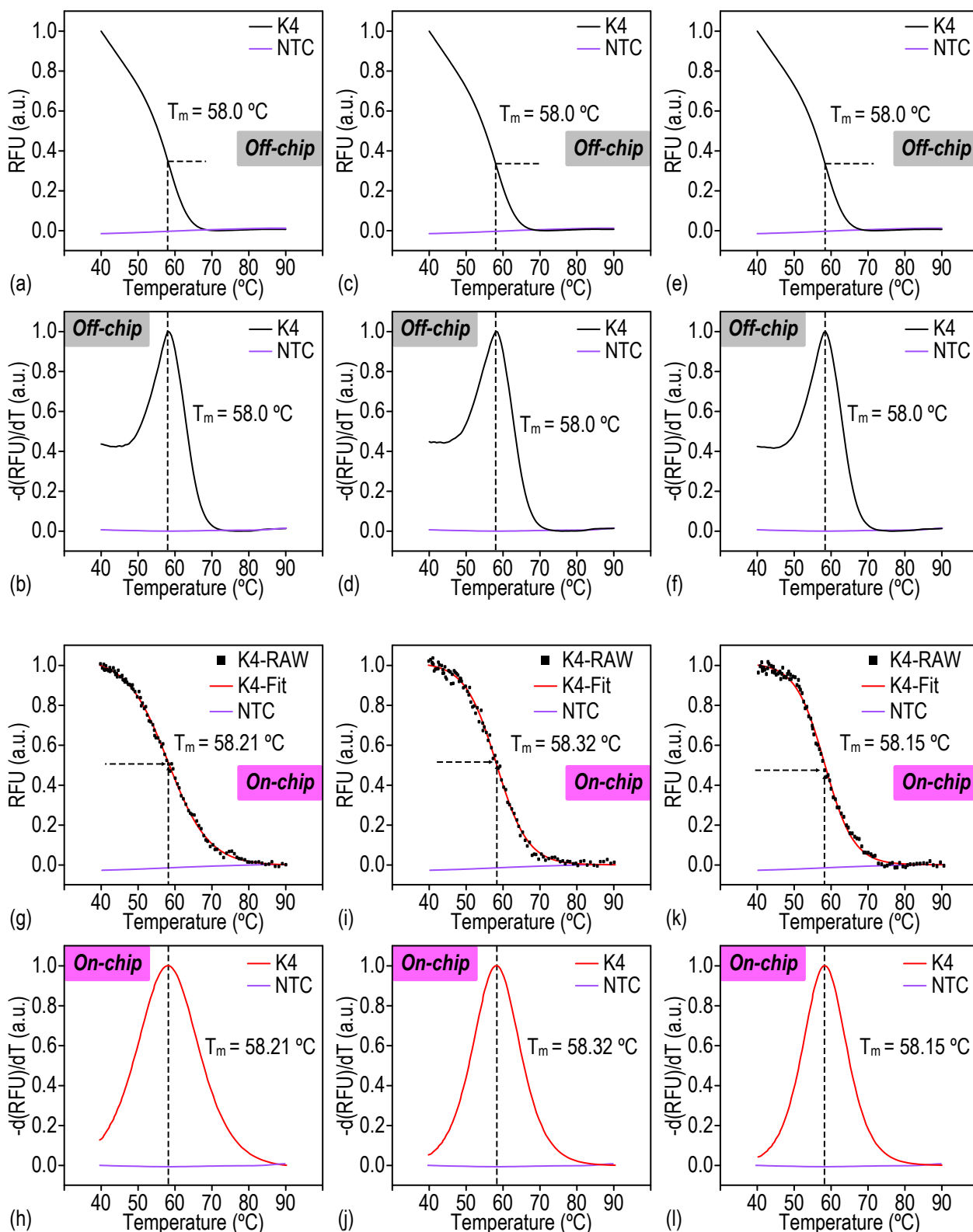
Figure S15. Experimental results illustrate the MCA tests for mutant-type KRAS gene target (K4). (a, c, e) the off-chip melting curves, and (g, i, k) the on-chip melting curves. (b, d, f) and (h, j, l) demonstrate the off-chip and on-chip melting peaks, respectively.